COMPDYN 2011
3rd ECCOMAS Thematic Conference on
Computational Methods in Structural Dynamics and Earthquake Engineering
M. Papadrakakis, M. Fragiadakis, V. Plevris (eds.)
Corfu, Greece, 25–28 May 2011

COMPUTATIONAL CONTACT DYNAMICS INCLUDING MULTIPHYSICS AND MULTISCALE EFFECTS

Alexander Popp and Wolfgang A. Wall

Institute for Computational Mechanics, Technische Universität München
Boltzmannstr. 15, 85748 Garching b. München, Germany
e-mail: {popp,wall}@lnm.mw.tum.de

Keywords: Contact Dynamics, Mortar Methods, Finite Deformations, Dual Lagrange Multipliers, Fluid-Structure Interaction with Contact, Finite Elements.

Abstract. *This paper gives a review of our recently proposed dual mortar approach combined with a consistently linearized semi-smooth Newton method for 3D finite deformation contact analysis. The mortar finite element method, which is applied as discretization scheme, initially yields a mixed formulation with the nodal Lagrange multiplier degrees of freedom as additional primary unknowns. However, by using so-called dual shape functions for Lagrange multiplier interpolation, the global linear system of equations to be solved within each Newton step can be condensed and thus contains only displacement degrees of freedom. All possible types of nonlinearities, including finite deformations, nonlinear material behavior and contact itself (active set search) are handled within one single iterative solution scheme based on a consistently linearized semi-smooth Newton method. The extension of the proposed framework towards additional model complexities such as Coulomb friction and self contact is addressed shortly. Moreover, an outlook towards multiphysics and multiscale simulations, coupling contact analysis with other physical fields and taking into account effects on different length scales is provided by exemplarily discussing the integration of mortar contact into a fixed-grid fluid-structure interaction (FSI) framework based on the extended finite element method (XFEM). Several numerical examples are presented to show the high quality of results obtained with the proposed methods.*

1 INTRODUCTION

Computational contact dynamics in general, and mortar-based discretization for finite deformations in particular, have seen a great thrust of research over the last decade. We discuss here the most important features of the recently proposed dual mortar finite element method combined with a consistently linearized semi-smooth Newton scheme for contact constraint enforcement. The present contribution is thus a shortened version of our articles [1, 2, 3, 4] to which we refer for full technical details, more profound discussion of the methods presented and further numerical examples.

Many newly proposed contact discretizations are based on the mortar method which was originally introduced in the context of domain decomposition [5]. Mortar contact formulations have successfully been applied to the solution of finite deformation contact problems in [6, 7, 8]. However, the mentioned formulations all apply a regularization of contact constraints based on the penalty method or an augmented Lagrangian type approach using the Uzawa algorithm. A recent application based on direct Lagrange multiplier techniques with standard multiplier spaces can be found in [9]. Yet, the dual Lagrange multiplier spaces proposed in [10, 11] seem to have the highest potential for efficient algorithms as they allow for a static condensation of the discrete Lagrange multiplier degrees of freedom. Thus, an undesirable increase in global system size, usually typical of direct Lagrange multiplier techniques, is avoided. Mortar methods with dual Lagrange multipliers have first been developed in the context of small deformation contact problems [12], where also the idea of interpreting the active set search as a semi-smooth Newton method (see e.g. [13, 14]) has been adapted. Some first steps towards a finite deformation implementation have been made in [15, 16], however still with an incomplete linearization of contact forces and constraints. In the authors' previous work [1, 2, 3], the ideas of dual Lagrange multipliers and a semi-smooth Newton approach for the active set search have been consistently extended to fully nonlinear 3D frictional contact problems.

Advantageous properties of the devised algorithms comprise superior robustness as compared with a traditional node-to-segment approach, the absence of any user-defined parameter (e.g. penalty parameter), the integration of all types of nonlinearities (including finite deformations, nonlinear material behavior and active set search) into one single iteration loop and the possibility to condense the discrete Lagrange multipliers from the global system of equations, to name only a few. First-order and second-order finite element interpolation, frictional sliding based on Coulomb's law as well as self contact are considered for both 2D and 3D. Some very challenging numerical examples are presented to illustrate the high quality of results obtained with the proposed approach. The design of our algorithms is based on overlapping domain decomposition, involving parallel contact search based on hierarchic binary tree structures and a novel dynamic load balancing strategy specifically developed for mortar coupling. This assures full parallel scalability of all algorithmic components when solving large contact dynamics problems with up to some million degrees of freedom.

Recently, the focus of our research in the field of computational contact dynamics has been extended towards multiphysics and multiscale simulations, coupling contact analysis with several other physical fields and taking into account effects on different length scales. Exemplarily, the integration of dual mortar contact into a fixed-grid fluid-structure interaction (FSI) framework based on the extended finite element method (XFEM) will be shortly addressed here. This approach allows for computing macroscopic contact of arbitrarily deforming structures embedded in a surrounding fluid. Again, we refer to a recent article [4] for the derivation and a more profound discussion of the proposed fluid-structure-contact interaction method.

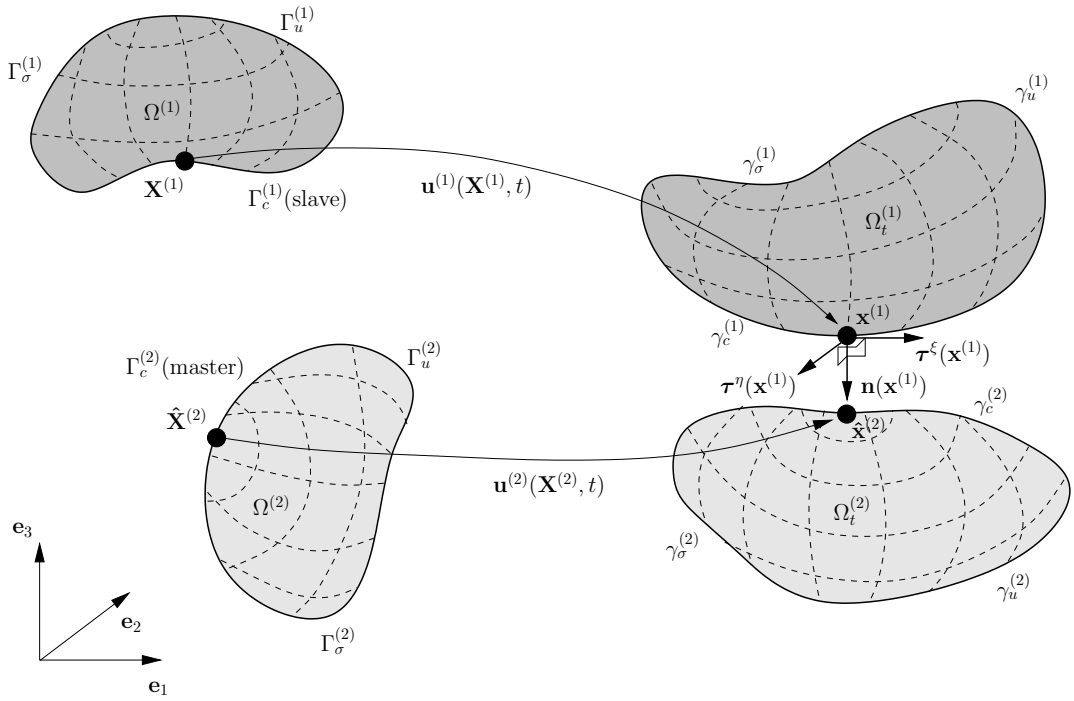

Figure 1: Notation for the two body finite deformation contact problem in 3D.

The remainder of this contribution is organized as follows: Section 2 provides a rough overview of the general continuum mechanics problem setup for 3D finite deformation contact. The dual mortar finite element approach is described in Section 3. In Section 4, the semi-smooth Newton type active set strategy and the resulting solution algorithm are outlined. Section 5 highlights some recent model extensions, including friction and fluid-structure-contact interaction. Following this interlude, Section 6 demonstrates with several numerical examples the validity of the proposed approach. Finally, we conclude the findings.

2 PROBLEM FORMULATION OF FINITE DEFORMATION CONTACT

The basic problem definition has been described in detail in [2]. Figure 1 shows the reference and current configurations of two elastic bodies undergoing a finite deformation process and introduces some notation. The surfaces $\partial\Omega_t^{(i)}$, $i=1,2$ are divided into three disjoint boundary sets, namely the common Dirichlet and Neumann boundaries $\gamma_u^{(i)}$ and $\gamma_\sigma^{(i)}$ as well as the potential contact surfaces $\gamma_c^{(i)}$. Although a mortar discretization will be applied later, we still retain the customary nomenclature of slave and master contact surfaces.

Displacement vectors $\mathbf{u}^{(i)} = \mathbf{x}^{(i)} - \mathbf{X}^{(i)}$ describe the motion of the deformable bodies from reference configuration $\mathbf{X}^{(i)}$ to current configuration $\mathbf{x}^{(i)}$. Material nonlinearity is taken into account by assuming a compressible Neo-Hookean material behavior based on the second Piola-Kirchhoff stress tensor $\mathbf{S}$ and the Green-Lagrange strain tensor $\mathbf{E} = \frac{1}{2}\left(\mathbf{F}^T\mathbf{F} - \mathbf{I}\right)$, where $\mathbf{F}$ is the deformation gradient. Based on these definitions, the well-known initial boundary value problem (IBVP) of finite deformation elastodynamics can be formulated. This paper focuses on contact interaction itself, which is typically described by a gap function $g(\mathbf{X},t)$ in the current configuration. The classical Karush-Kuhn-Tucker (KKT) conditions of normal contact and the

frictionless sliding conditions then read as follows:

$$g(\mathbf{X},t) \geq 0 \, , \;\; p_n \leq 0 \, , \;\; p_n \, g(\mathbf{X},t) = 0 \, , \tag{1}$$

$$t_\tau^\xi = t_\tau^\eta = 0 \, , \tag{2}$$

where the normal and tangential components of the slave contact traction $\mathbf{t}_c^{(1)}$ are denoted as p_n, t_τ^ξ and t_τ^η. A corresponding formulation of Coulomb's law for frictional contact is omitted here, but can be found in our recent work [3]. For deriving a weak formulation the solution space $\mathscr{U}^{(i)}$ and the weighting space $\mathscr{V}^{(i)}$ are defined by employing the usual Sobolev spaces $H^1\left(\Omega^{(i)}\right)$ and by taking into acccount Dirichlet boundary conditions. The method of weighted residuals then yields: Find $u_j^{(i)} \in \mathscr{U}^{(i)}$ such that

$$\delta\Pi\left(\mathbf{u},\delta\mathbf{u},\boldsymbol{\lambda}\right) = \delta\Pi_{int,ext}\left(\mathbf{u},\delta\mathbf{u}\right) + \int_{\gamma_c^{(1)}} \boldsymbol{\lambda} \cdot \left(\delta\mathbf{u}^{(1)} - \delta\hat{\mathbf{u}}^{(2)}\right) \mathrm{d}\gamma = 0$$

$$\forall \, \delta u_j^{(i)} \in \mathscr{V}^{(i)} \, , \;\; j = 1,2,3 \, , \tag{3}$$

where the negative contact traction on the slave side of the interface has been replaced by a Lagrange multiplier vector $\boldsymbol{\lambda} = -\mathbf{t}_c^{(1)}$. By arbitrary choice, the Lagrange multipliers $\lambda_j \in \mathscr{M}$, $j = 1,2,3$, have been introduced on the slave side, where $\mathscr{M}$ is defined as dual space of the trace space $\mathscr{W}^{(1)}$ of $\mathscr{U}^{(1)}$ restricted to $\Gamma_c^{(1)}$. Corresponding test functions $\delta\lambda_j$ serve as weighting functions for the non-penetration constraint in (1):

$$\int_{\gamma_c^{(1)}} \delta\lambda_n \, g(\mathbf{X},t) \, \mathrm{d}\gamma \geq 0 \qquad \forall \, \delta\lambda_n \in \mathscr{M} \, . \tag{4}$$

The remaining contact conditions in (1) and (2) are then rewritten as

$$\lambda_n \geq 0 \, , \;\; \lambda_n \, g(\mathbf{X},t) = 0 \, , \;\; \lambda_\tau^\xi = \lambda_\tau^\eta = 0 \, . \tag{5}$$

Altogether, equations (3)–(5) establish a mixed variational formulation with the solution $u_j^{(i)} \in \mathscr{U}^{(i)}$ and $\lambda_j \in \mathscr{M}$. An overview of mortar finite element discretization using dual Lagrange multipliers follows in the upcoming paragraph. Some of the contact constraints are still formulated as inequality conditions, which necessitates the application of a suitable active set strategy. The primal-dual active set strategy (PDASS) and our reformulation as a semi-smooth Newton scheme including consistent linearization will be addressed in Section 4.

3 DUAL MORTAR FINITE ELEMENT DISCRETIZATION

Spatial discretization of the contact terms requires a discretization of slave and master surface, which is directly connected to the underlying structural discretization based on their trace space relationship. We consider both first-order and second-order Lagrangian finite elements in 2D and 3D. A general definition of slave and master displacements then reads as follows:

$$\mathbf{d}^{(1)h}\big|_{\Gamma_c^{(1)h}} = \sum_{k=1}^{n_{sl}} N_k^{(1)}(\boldsymbol{\xi}^{(1)}) \, \mathbf{d}_k^{(1)} \, , \quad \mathbf{d}^{(2)h}\big|_{\Gamma_c^{(2)h}} = \sum_{l=1}^{n_m} N_l^{(2)}(\boldsymbol{\xi}^{(2)}) \, \mathbf{d}_l^{(2)} \, . \tag{6}$$

Spatially discretized quantities are labeled with a superscript h and the total number of slave and master nodes is n_{sl} and n_m, respectively. Nodal displacements are given by $\mathbf{d}_k^{(1)}$, $\mathbf{d}_l^{(2)}$ and

shape functions $N_k^{(1)}$, $N_l^{(2)}$ are defined with respect to the usual finite element parameter spaces $\boldsymbol{\xi}^{(i)}$. Lagrange multiplier interpolation is based on dual shape functions Φ_j, as pioneered by Wohlmuth [10]:

$$\boldsymbol{\lambda}^h = \sum_{j=1}^{n_{sl}} \Phi_j(\boldsymbol{\xi}^{(1)})\, \mathbf{z}_j \,, \tag{7}$$

with discrete nodal Lagrange multipliers $\mathbf{z}_j$. The construction of dual shape functions is based on a biorthogonality relation as introduced in [10, 11, 12]:

$$\int_{\gamma_c^{(1)h}} \Phi_j(\boldsymbol{\xi}^{(1)})\, N_k^{(1)}(\boldsymbol{\xi}^{(1)})\, \mathrm{d}\gamma = \delta_{jk} \int_{\gamma_c^{(1)h}} N_k^{(1)}(\boldsymbol{\xi}^{(1)})\, \mathrm{d}\gamma \,, \tag{8}$$

where δ_{jk} is the Kronecker delta. This approach will later allow for static condensation of the discrete multipliers $\mathbf{z}_j$. Note, that in the context of finite deformations dual shape functions become deformation-dependent themselves. For an overview and exemplary local calculations of element-specific dual shape functions in 2D and 3D contact analysis we refer to [1, 2, 15]. Nodal blocks of the two mortar integral matrices $\mathbf{D} \in \mathbb{R}^{3n_{sl}\times 3n_{sl}}$ and $\mathbf{M} \in \mathbb{R}^{3n_{sl}\times 3n_m}$ are then defined as

$$\mathbf{D}[j,k] = D_{jk}\,\mathbf{I}_3 = \delta_{jk} \int_{\gamma_c^{(1)h}} N_k^{(1)} \mathrm{d}\gamma\, \mathbf{I}_3 \,, \tag{9}$$

$$\mathbf{M}[j,l] = M_{jl}\,\mathbf{I}_3 = \int_{\gamma_c^{(1)h}} \Phi_j N_l^{(2)} \mathrm{d}\gamma\, \mathbf{I}_3 \,, \tag{10}$$

with $j,k = 1,...,n_{sl}$, $l = 1,...,n_m$ and with the identity $\mathbf{I}_3 \in \mathbb{R}^{3\times 3}$. Owing to the biorthogonality relation (8), $\mathbf{D}$ reduces to a diagonal matrix. This yields as algebraic notation of the discretized contact virtual work

$$\delta\Pi_c^h = \left(\delta\mathbf{d}^{(1)}\right)^T \mathbf{D}^T\mathbf{z} - \left(\delta\mathbf{d}^{(2)}\right)^T \mathbf{M}^T\mathbf{z}, \tag{11}$$

where all discrete nodal values of Lagrange multipliers and nodal test function values are assembled into global vectors $\mathbf{z}$, $\delta\mathbf{d}^{(1)}$ and $\delta\mathbf{d}^{(2)}$, respectively. For the ease of notation, the set of all finite element nodes is now split into three subsets: a subset $\mathscr{S}$ containing all n_{sl} potential slave side contact nodes, a subset $\mathscr{M}$ of all n_m potential master side contact nodes and the set of all remaining nodes $\mathscr{N}$. The global displacement vector can be sorted accordingly, yielding $\mathbf{d} = (\mathbf{d}_{\mathscr{N}}, \mathbf{d}_{\mathscr{M}}, \mathbf{d}_{\mathscr{S}})^T$. Then, the vector of discrete contact forces is

$$\mathbf{f}_c = \begin{bmatrix}\mathbf{0} & -\mathbf{M} & \mathbf{D}\end{bmatrix}^T \mathbf{z} \,. \tag{12}$$

The contact forces extend the fully discretized force residual resulting from standard finite element discretization of internal and external virtual work in (3). This yields the total nonlinear force residual

$$\mathbf{r} := \mathbf{f}_{int}(\mathbf{d}) - \mathbf{f}_{ext} + \mathbf{f}_c(\mathbf{d},\mathbf{z}) = 0 \,. \tag{13}$$

A discrete version of the weak non-penetration condition is obtained by inserting the Lagrange multiplier interpolation (7) into (4)

$$\int_{\gamma_c^{(1)}} \delta\lambda_n\, g\, \mathrm{d}\gamma \approx \sum_{j=1}^{n_{sl}} (\delta z_n)_j \int_{\gamma_c^{(1)h}} \Phi_j\, \hat{g}\, \mathrm{d}\gamma := \sum_{j=1}^{n_{sl}} (\delta z_n)_j\, \tilde{g}_j \geq 0 \,. \tag{14}$$

Here, $\hat{g}$ is the discrete version of the gap function, and for each slave node $j \in \mathscr{S}$ a discrete normal weighted gap $\tilde{g}_j$ has been introduced. Discretization of the remaining contact conditions yields as discrete formulation of the KKT conditions and the frictionless sliding conditions:

$$\tilde{g}_j \geq 0\,, \;\; (z_n)_j \geq 0\,, \;\; (z_n)_j \tilde{g}_j = 0\,, \tag{15}$$

$$(z_\tau^\xi)_j = (z_\tau^\eta)_j = 0\,. \tag{16}$$

It is worth mentioning that although a mortar discretization has been employed, the weighted constraints at discrete nodal points are enforced independently.

4 SOLUTION ALGORITHM

In our recent papers [1, 2, 3] the active set search has been successfully applied as a semi-smooth Newton method to both 2D and 3D finite deformation contact analysis. The main advantage of this new approach is the fact that all sources of nonlinearities, i.e. finite deformations, nonlinear material behavior and contact itself, can be efficiently treated within one single iterative scheme. The basic idea is a simple reformulation of the discrete KKT conditions in (15) within a so-called nonlinear complementarity function C_j for each slave node $j \in \mathscr{S}$:

$$C_j\left(\mathbf{z}_j, \mathbf{d}\right) = (z_n)_j - \max\left(0, (z_n)_j - c_n \tilde{g}_j\right) = 0\,, \;\; c_n > 0\,. \tag{17}$$

It can be easily shown that (17) is equivalent to the set of KKT conditions and that this equivalence holds for arbitrary positive values of the purely algorithmic complementarity parameter c_n. While C_j is a continuous function, it is non-smooth and has no uniquely defined derivative at positions $(z_n)_j - c_n \tilde{g}_j = 0$. Yet, it is well-known from mathematical literature on constrained optimization [14] and from applications in small deformation contact analysis [12] that the *max*-function is semi-smooth and therefore a Newton method can still be applied. Deriving a consistent Newton method for the iterative solution of the nonlinear contact problem under consideration relies on the full linearization of all deformation-dependent quantities, such as nodal normal and tangential vectors or mortar integral matrices. This linearization process has been presented in great detail for both 2D and 3D case in [1, 2]. The resulting algorithm to be solved within one time increment is summarized next. All types of nonlinearities including the search for the correct active set are resolved within one Newton iteration, with the active and incative sets $\mathscr{A}$ and $\mathscr{I}$ being updated after each semi-smooth Newton step:

Algorithm 1

1. Set $i = 0$ and initialize the solution $(\mathbf{d}_0, \mathbf{z}_0)$.
2. Initialization: $\mathscr{A}_0 \cup \mathscr{I}_0 = \mathscr{S}$ and $\mathscr{A}_0 \cap \mathscr{I}_0 = \emptyset$.
3. Find the primal-dual pair $(\Delta\mathbf{d}_i, \mathbf{z}_{i+1})$ by solving

$$\Delta\mathbf{r}|_i = -\mathbf{r}|_i\,, \tag{18}$$

$$\mathbf{z}_j|_{i+1} = 0 \qquad \forall\, j \in \mathscr{I}_i\,, \tag{19}$$

$$\Delta\tilde{g}_j|_i = -\tilde{g}_j|_i \qquad \forall\, j \in \mathscr{A}_i\,, \tag{20}$$

$$\Delta\boldsymbol{\tau}_j^{\xi/\eta} \cdot \mathbf{z}_j|_i + \boldsymbol{\tau}_j^{\xi/\eta} \cdot \mathbf{z}_j|_{i+1} = 0 \qquad \forall\, j \in \mathscr{A}_i\,. \tag{21}$$

4. Update $\mathbf{d}_{i+1} = \mathbf{d}_i + \Delta\mathbf{d}_i$.

5. Set $\mathscr{A}_{i+1}$ and $\mathscr{I}_{i+1}$ to

$$\mathscr{A}_{i+1} := \left\{ j \in \mathscr{S} \,|\, (z_n)_j|_{i+1} - c_n \tilde{g}_j|_{i+1} > 0 \right\} ,$$
$$\mathscr{I}_{i+1} := \left\{ j \in \mathscr{S} \,|\, (z_n)_j|_{i+1} - c_n \tilde{g}_j|_{i+1} \leq 0 \right\} . \tag{22}$$

6. If $\mathscr{A}_{i+1} = \mathscr{A}_i$, $\mathscr{I}_{i+1} = \mathscr{I}_i$ and $\|\mathbf{r}_{tot}\| \leq \varepsilon_r$, then stop,
   else set $i := i+1$ and go to step (3).

Here, ε_r represents an absolute Newton convergence tolerance for the L2-norm of the total residual vector $\mathbf{r}_{tot}$, which comprises the force residual $\mathbf{r}$ and the residual of the contact constraints (19)–(21). Numerous tests reveal that even for large step sizes and fine contacting meshes the correct active set is found after a few Newton steps. Once the sets remain constant, quadratic convergence is obtained due to the underlying consistent linearization. Owing to the dual Lagrange multiplier shape functions, the mortar matrix $\mathbf{D}$ becomes diagonal, which makes its inversion trivial. Thus, the discrete multiplier values are eliminated by condensation and the resulting linear system of equations is not of saddle point type anymore but contains only displacement degrees of freedom. Here, we restrict the presentation to a schematic form

$$\mathbf{L}_{dd}|_i \, \Delta \mathbf{d}_i = -\tilde{\mathbf{r}}_{tot}|_i \, , \tag{23}$$

which illustrates the modified residual vector $\tilde{\mathbf{r}}_{tot}$ emanating from $\mathbf{r}_{tot}$ by condensation of the discrete Lagrange multiplier degrees of freedom. Similarly, we obtain a modified effective tangent stiffness matrix $\mathbf{L}_{dd}$ including contact stiffness and condensed constraint terms.

5 RECENT EXTENSIONS OF THE PROPOSED METHODS

In this section, some recent extensions of the methods described above are outlined. This includes efficient parallel implementation, the treatment of self contact and Coulomb friction as well as the consistent integration of mortar contact into an XFEM based fixed-grid fluid-structure interaction framework.

5.1 Efficient parallel implementation and self contact

The solution of finite deformation contact problems is difficult to be managed due to the strong nonlinearities involved. A brute force approach for contact search may add another very time-consuming part, which is why efficient parallel search algorithms are needed. Here, we employ a recently developed approach [17] based on so-called discretized-orientation-polytopes (k-DOPs) as bounding volumes. Compared to the common axis-aligned bounding boxes, the k-DOPs allow for a much tighter and thus more efficient geometrical representation of the contact surfaces. Slave and master contact surface are organized within hierarchical binary tree structures so that very fast search and tree update procedures can be applied. The approach given in [17] for the single-processor case has been extended to fit into a parallel finite element simulation framework based on overlapping domain decomposition. An extension to self contact is presented in [18] and has also been included into our simulation framework. The search algorithm again is based on a bounding volume hierarchy organized as a binary tree. It is however crucial for self contact simulations to set up the bounding volume hierarchy in a *bottom-up* way based on mesh connectivity (e.g. using a dual graph). Moreover, a curvature criterion may be used to accelerate the searching procedure. Finally, dynamic assignment of slave and master sub-surfaces, which are unknown *a priori* for self contact problems, becomes necessary.

In addition, we make use of a novel strategy for dynamic load balancing specifically developed for mortar-based interface coupling. Within each time step the evaluation of contact integrals is adaptively distributed among all processors, so that an optimal balance of processor workload is obtained. Parallel (self) contact search and dynamic load balancing together assure the parallel scalability of all presented algorithmic components even when solving large contact dynamics problems with up to some million degrees of freedom.

5.2 Treatment of friction

An extension of the described mortar contact algorithms to the 2D frictional case has recently been proposed [3]. All steps outlined in Sections 2-4 remain conceptually unchanged. Only the frictionless sliding conditions introduced in (2) are replaced by frictional sliding conditions, e.g. using Coulomb's law. Based on an objective formulation of friction kinematic variables [8] the additional constraints again are recast into non-smooth nonlinear complementarity functions, as presented for the non-penetration constraint in (17). By applying full linearization, the frictional constraints are consistently integrated into the semi-smooth Newton scheme. All nonlinearities, now additionally including friction (i.e. search for the current stick and slip regions), are again treated within one single iterative scheme. For further details and numerical examples, the interested reader is referred to [3].

5.3 Fluid-structure-contact interaction

Finite deformation contact of flexible solids embedded in fluid flows occurs in a wide range of engineering scenarios. We recently proposed a novel three-dimensional finite element approach in order to tackle this problem class [4]. The method consists of the dual mortar contact formulation presented above, which is algorithmically integrated into an extended finite element method (XFEM) fluid-structure interaction approach [19, 20]. The combined fluid-structure-contact interaction method (FSCI) allows to compute contact of arbitrarily moving and deforming structures embedded in an arbitrary flow field. In [4], the fluid is described by instationary incompressible Navier-Stokes equations. An interface handling algorithm [21] is applied to obtain an exact fluid-structure interface representation, which permits to capture flow patterns around contacting structures very accurately as well as to simulate dry contact between structures. No restrictions arise for the structural and the contact formulation. A linearized monolithic system of equations can be derived, which contains the fluid formulation, the structural formulation, the contact formulation as well as the coupling conditions at the fluid-structure interface. This linearized system may then be solved either by partitioned or by monolithic fluid-structure coupling algorithms.

6 NUMERICAL EXAMPLES

We present three numerical examples to illustrate the capabilities of the proposed approach. All simulations are based on a parallel implementation of the contact and FSCI algorithms described above in our in-house multiphysics research code BACI [22]. A compressible Neo-Hookean constitutive law determined by Young's modulus E and Poisson's ratio ν is employed for all structures. Convergence of a Newton iterative scheme is measured in terms of the total residual norm with a relative convergence tolerance of 10^{-12}. The complementarity parameter described in Section 4 is set to $c_n = 1$, which guarantees for all problem setups considered that the correct active set is found within only a few semi-smooth Newton steps.

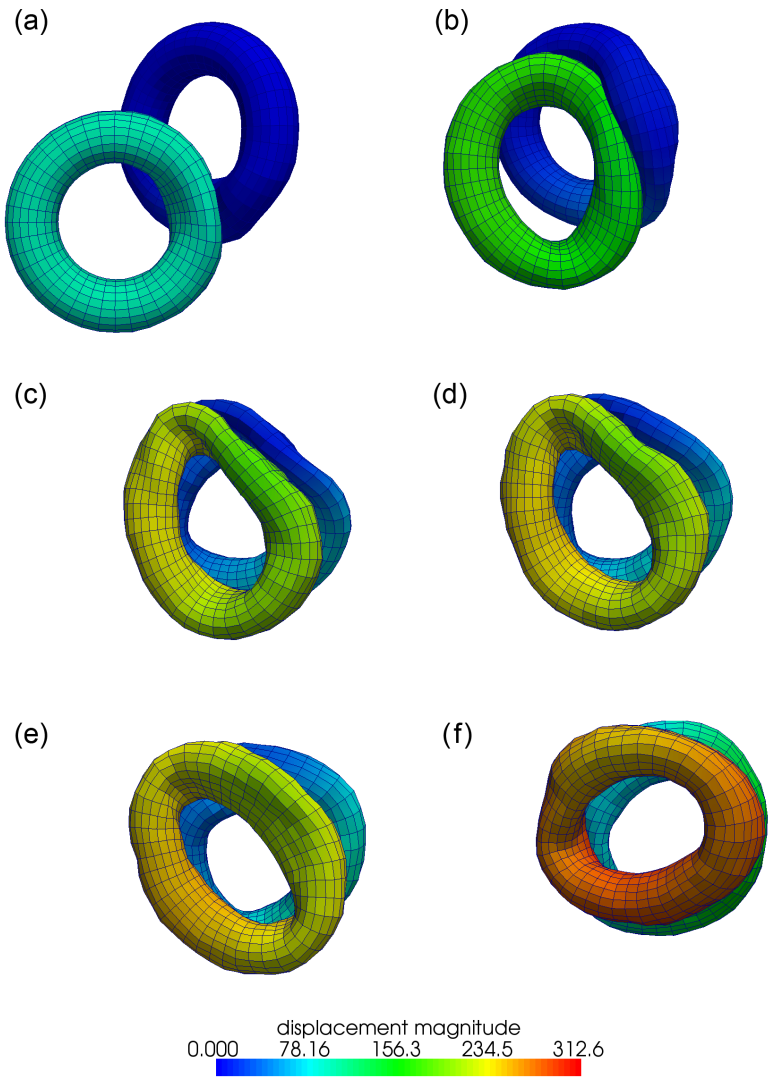

Figure 2: Two torus impact – displacement magnitude at characteristic stages of deformation: (a) $t = 3$; (b) $t = 5$; (c) $t = 7$; (d) $t = 7.5$; (e) $t = 8$; (f) $t = 10$.

6.1 Two torus impact

In this example, a finite deformation impact problem of two toruses ($E = 2250$, $\nu = 0.3$) is investigated. Both geometry and loading conditions are based on a quite similar analysis presented in [17] to evaluate contact search strategies. The finite element mesh consists of 1600 8-node hexahedral elements in total. The major and minor radius of the two hollow toruses is 76 and 24, repectively and the wall thickness is 4.5. The upper torus is rotated around the vertical axis by 45 degrees. We apply transient structural dynamics here using a Generalized-α time integration scheme [23] with the density of the contacting bodies chosen as $\rho = 0.1$.

During a total of 200 time steps (step size $\Delta t = 0.05$) the lower torus is first accelerated towards the upper torus and then a very general oblique impact situation with large structural deformations occurs. In addition to that, the proposed method needs to resolve continuous changes of the active contact set due to the large amount of (frictionless) sliding. Figure 2 shows six characteristic deformed configurations associated with the simulation stages described above.

Table 1 illustrates convergence of the presented fully linearized semi-smooth Newton scheme in terms of the total residual norm for two representative time steps both including large defor-

Newton step	*(a)* $t = 4.5$	*(b)* $t = 5.5$
1	1.09e+06 (*)	1.04e+06 (*)
2	2.16e+04 (*)	3.60e+04 (*)
3	4.05e+00	1.38e+01 (*)
4	1.53e−04	2.11e−03
5	2.46e−08	2.77e−08

(*) = change in active contact set

Table 1: Convergence behavior of the proposed semi-smooth Newton scheme in terms of the total residual norm for two representative time steps $\Delta t = 0.05$ starting from (a) $t = 4.5$ and (b) $t = 5.5$.

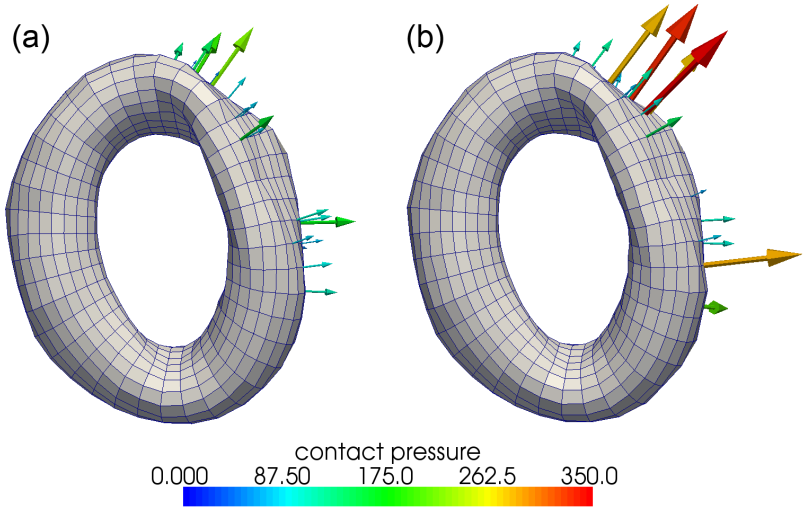

Figure 3: Two torus impact – exemplary visualization of the deformed lower torus and of the computed contact traction results at (a) $t = 5.5$ and (b) $t = 5.55$.

mations and considerable changes of the active contact set. The results demonstrate that the semi-smooth Newton method features excellent convergence in this example. The integration of all types of nonlinearities into a semi-smooth Newton scheme avoids tremendous computational cost as compared with a fixed-point type approach for the active set (see e.g. [9, 16]). Moreover, it is obvious that consistent linearization of all nonlinear quantities, including contact forces, normal and tangential vectors, is crucial to avoid deterioration of convergence.

To illustrate the strong nonlinearities involved in this problem setup even more clearly, Figure 3 shows the deformed lower torus at the beginning and at the end of the time step analyzed in column (b) of Table 1 (i.e. at $t = 5.5$ and at $t = 5.55$). The normal contact traction distribution, represented by the nodal Lagrange multiplier solution, is visualized with arrows and confirms that despite significant changes of the contact region, all nonlinearities are resolved efficiently and without deterioration of convergence within one single semi-smooth Newton iteration.

6.2 Hollow sphere pushed through elastic tube

In this example, a hollow sphere ($E = 500$, $\nu = 0.3$) is pushed through a tube ($E = 1000$, $\nu = 0.3$). Geometrical setup and finite element mesh based on 8-node hexahedral elements are depicted in Figure 4. Due to the application of a load-controlled scheme in combination with the frictionless sliding case considered, the deformation cannot be resolved by a quasistatic simulation. Thus, again transient structural dynamics is applied using Generalized-α time inte-

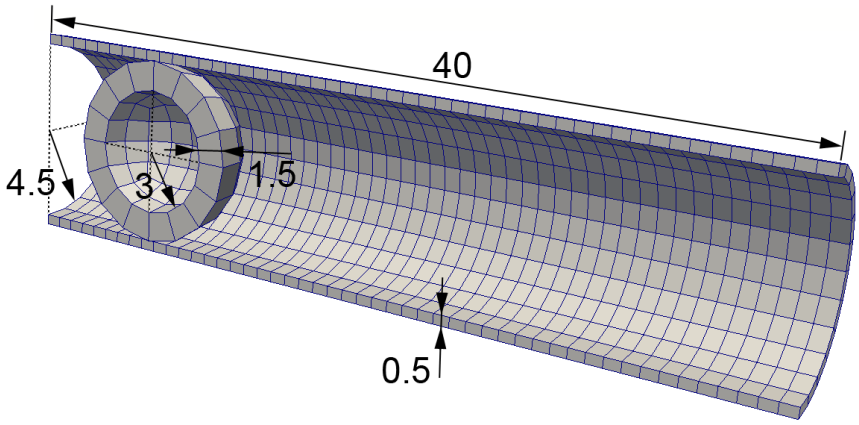

Figure 4: Sphere pushed through tube – geometry and finite element mesh.

Step	*(a)* during inflation	*(b)* during pushing
1	3.08e+00 (*)	3.39e+01 (*)
2	1.10e+00	4.80e+00 (*)
3	6.82e−03	3.35e−02 (*)
4	6.74e−08	5.62e−06
5	5.04e−11	4.87e−11

(*) = change in active contact set

Table 2: Convergence behavior of the proposed semi-smooth Newton scheme in terms of the total residual norm for two representative time steps during (a) inflation (steps 1–20) and (b) pushing (steps 21–40).

gration with the density of the contacting bodies chosen as $\rho = 7.8 \cdot 10^{-6}$. During a total of 40 time steps, we first inflate the hollow sphere by internal pressure (steps 1–20) and then push it along the axial direction of the tube (steps 21–40). Figure 5 shows two deformed configurations associated with the two stages described above.

Table 2 illustrates convergence in terms of the total residual norm for two representative time steps during inflation of the hollow sphere and during pushing. Again, for this transient contact simulation of two elastic bodies, the presented algorithm is capable of efficiently solving all types of nonlinearities including active set search within one semi-smooth Newton scheme.

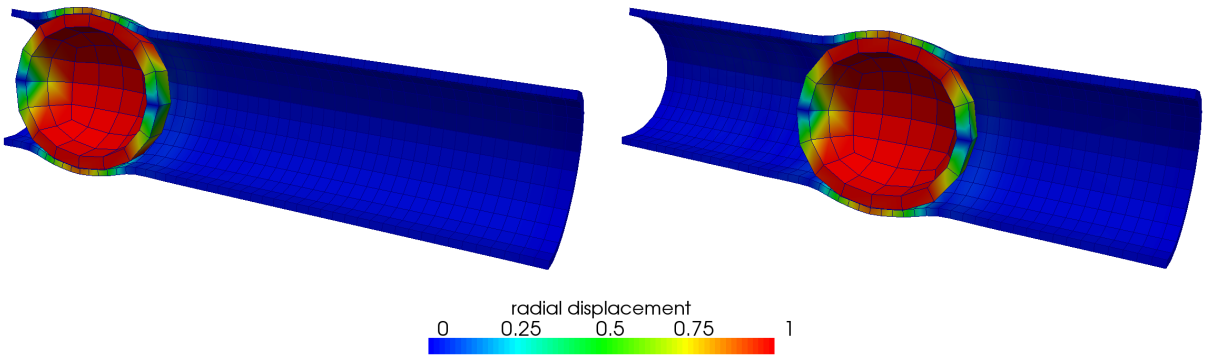

Figure 5: Sphere pushed through tube – characteristic stages of deformation.

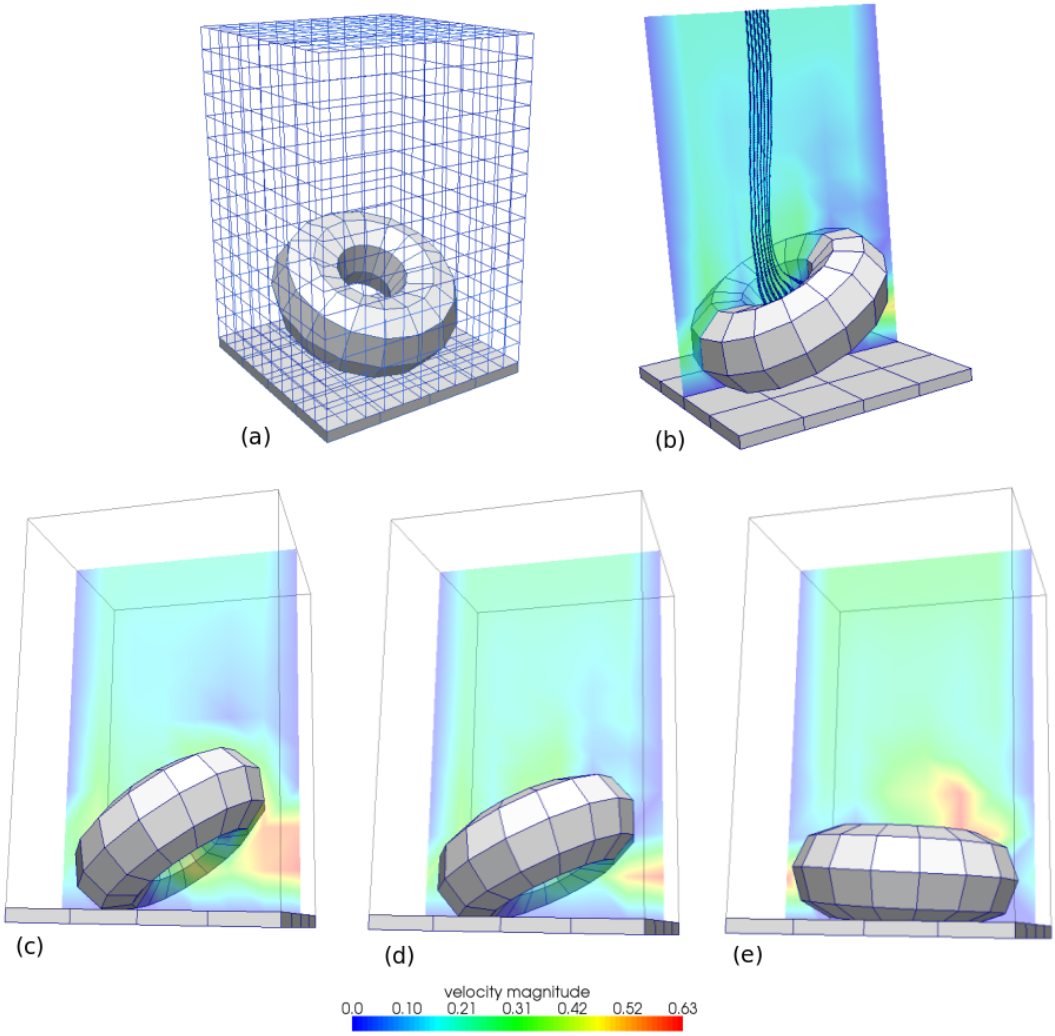

Figure 6: 3D torus contacting a stiff wall – (a) finite element mesh, (b) stream lines through the inner hole of the torus before contact (c)–(e) fluid velocity and structural movement are visualized for several time steps of the dynamic fluid-structure-contact interaction process.

6.3 Fluid-structure-contact interaction: elastic torus

The third test case illustrates a three-dimensional fluid-structure-contact interaction example. An elastic torus ($E = 4000$, $\nu = 0.4$) rotated around a horizontal axis by an angle of 65 degrees is placed in a 3D channel as depicted in Figure 6. A parabolic inflow profile is imposed at the top boundary of the channel and zero traction Neumann boundaries allow outflow on the left and right side near the bottom. All other channel boundaries are no-slip boundaries. Both the structural and the fluid mesh consist of 8-node hexahedral elements, with state-of-the-art stabilization techniques being used in the fluid elements. The velocity field around the moving torus is depicted in Figure 6. Stream lines illustrate the 3D fluid flow through the inner hole of the torus before contacting with the wall. At first, the torus is moving towards the wall due to the interaction with the fluid stresses. The exact interface representation allows to resolve flow patterns around the torus very close to contact and to simulate dry contact. After some time, the torus touches the wall and its further movement and deformation is influenced by the fluid at the fluid-structure interface and by contact forces at the contact interface.

7 CONCLUSIONS

The dual mortar method recently proposed by the authors for 3D finite deformation contact analysis has been reviewed and some important extensions have been highlighted. Consistent linearization of contact forces and constraints together with an interpretation of the active set search as a semi-smooth Newton scheme yields a very efficient solution algorithm. The accuracy of the presented method and its superior numerical robustness and efficiency have been demonstrated with several examples including finite deformations.

The integration of dual mortar contact into a fixed-grid fluid-structure interaction (FSI) framework based on the extended finite element method (XFEM) has been addressed shortly. This can be seen as a first step towards multiphysics and multiscale simulations, which couple contact analysis with several other physical fields and take into account effects on different length scales. Future work in this field will also focus on modeling finite deformation contact between slender beams and coupled thermomechanical contact, with applications ranging from Brownian dynamics of polymers in fiber networks to heat conduction and mechanical dissipation due to frictional sliding in turbine blade-to-disc joints.

REFERENCES

[1] A. Popp, M.W. Gee, W.A. Wall, A finite deformation mortar contact formulation using a primal-dual active set strategy. *International Journal for Numerical Methods in Engineering*, **79**, 1354–1391, 2009.

[2] A. Popp, M. Gitterle, M.W. Gee, W.A. Wall, A dual mortar approach for 3D finite deformation contact with consistent linearization. *International Journal for Numerical Methods in Engineering*, **83**, 1428–1465, 2010.

[3] M. Gitterle, A. Popp, M.W. Gee, W.A. Wall, Finite deformation frictional mortar contact using a semi-smooth Newton method with consistent linearization. *International Journal for Numerical Methods in Engineering*, **84**, 543–571, 2010.

[4] U. Mayer, A. Popp, A. Gerstenberger, W.A. Wall, 3D fluid-structure-contact interaction based on a combined XFEM FSI and dual mortar contact approach. *Computational Mechanics*, **46**, 53–67, 2010.

[5] C. Bernardi, Y. Maday, A.T. Patera, A new nonconforming approach to domain decomposition: the mortar element method. H. Brezis, J.L. Lions eds. *Nonlinear partial differential equations and their applications*, Pitman/Wiley: London/New York, 1994.

[6] M.A. Puso, T.A. Laursen, A mortar segment-to-segment contact method for large deformation solid mechanics. *Computer Methods in Applied Mechanics and Engineering*, **193**, 601–629, 2004.

[7] M.A. Puso, T.A. Laursen, A mortar segment-to-segment frictional contact method for large deformations. *Computer Methods in Applied Mechanics and Engineering*, **193**, 4891–4913, 2004.

[8] B. Yang, T.A. Laursen, X. Meng, Two dimensional mortar contact methods for large deformation frictional sliding. *International Journal for Numerical Methods in Engineering*, **62**, 1183–1225, 2005.

[9] C. Hesch, P. Betsch, A mortar method for energy-momentum conserving schemes in frictionless dynamic contact problems. *International Journal for Numerical Methods in Engineering*, **77**, 1468–1500, 2009.

[10] B.I. Wohlmuth, A mortar finite element method using dual spaces for the Lagrange multiplier. *SIAM Journal on Numerical Analysis*, **38**, 989–1012, 2000.

[11] B.I. Wohlmuth, *Discretization methods and iterative solvers based on domain decomposition*. Springer-Verlag Berlin Heidelberg, 2001.

[12] S. Hüeber, B.I. Wohlmuth, A primal-dual active set strategy for non-linear multibody contact problems. *Computer Methods in Applied Mechanics and Engineering*, **194**, 3147–3166, 2005.

[13] P.W. Christensen, A. Klarbring, J.S. Pang, N. Strömberg, Formulation and comparison of algorithms for frictional contact problems. *International Journal for Numerical Methods in Engineering*, **42**, 145–173, 1998.

[14] M. Hintermüller, K. Ito, K. Kunisch, The primal-dual active set strategy as a semismooth Newton method. *SIAM Journal on Optimization*, **13**, 865–888, 2002.

[15] S. Hartmann. *Kontaktanalyse dünnwandiger Strukturen bei grossen Deformationen*. PhD thesis, Institut für Baustatik und Baudynamik, Universität Stuttgart, 2007.

[16] S. Hartmann, S. Brunssen, E. Ramm, B. Wohlmuth, Unilateral non-linear dynamic contact of thin-walled structures using a primal-dual active set strategy. *International Journal for Numerical Methods in Engineering*, **70**, 883–912, 2007.

[17] B. Yang, T.A. Laursen, A contact searching algorithm including bounding volume trees applied to finite sliding mortar formulations. *Computational Mechanics*, **41**, 189–205, 2008.

[18] B. Yang, T.A. Laursen, A large deformation mortar formulation of self contact with finite sliding. *Computer Methods in Applied Mechanics and Engineering*, **197**, 756–772, 2008.

[19] A. Gerstenberger, W.A. Wall, An extended finite element method/Lagrange multiplier based approach for fluid-structure interaction. *Computer Methods in Applied Mechanics and Engineering*, **197**, 1699–1714, 2008.

[20] A. Gerstenberger, W.A. Wall, An embedded Dirichlet formulation for 3D continua. *International Journal for Numerical Methods in Engineering*, **82**, 537–563, 2010.

[21] U.M. Mayer, A. Gerstenberger, W.A. Wall, Interface handling for three-dimensional higher-order XFEM computations in fluid-structure interaction. *International Journal for Numerical Methods in Engineering*, **79**, 846–869, 2009.

[22] W.A. Wall, M.W. Gee. Baci - a multiphysics simulation environment. Technical report, Technische Universität München, 2010.

[23] J. Chung, G.M. Hulbert, A time integration algorithm for structural dynamics with improved numerical dissipation: the generalized-alpha method. *Journal of Applied Mechanics*, **60**, 371–375, 1993.